Predicting unstable toughness of concrete based on initial toughness criterion[*]

Long-bang QING[†1,2], Wen-ling TIAN[†‡1,2], Juan WANG[3]

(*1College of Civil Engineering, Hebei University of Technology, Tianjin 300401, China*)
(*2Civil Engineering Technology Research Center of Hebei Province, Tianjin 300401, China*)
(*3College of Water Conservancy and Environment Engineering, Zhengzhou University, Zhengzhou 450001, China*)
[†]E-mail: qlongbang@126.com; hebut_tm@163.com
Received Aug. 8, 2013; Revision accepted Nov. 5, 2013; Crosschecked Jan. 14, 2014

Abstract: The fracture processes of concrete were described by a cohesive crack model based on initial toughness criterion. The corresponding analytical method to predict the instability state was proposed. In this model, the initial toughness was adopted as the crack propagation criterion and the weight function method was used to calculate the stress intensity factor and the crack opening displacement caused by the cohesive stress. The unstable toughness can be easily obtained using the proposed method without measuring parameters at the critical state that was necessary in traditional methods. The proposed method was verified by existing experimental data of wedge splitting specimens with different grades of concrete and the sensitivity of the results on the tensile softening curve was discussed. The results demonstrate that the proposed method can well predict the peak load, the critical effective crack length, and the unstable toughness of concrete specimens. Moreover, the calculated unstable toughness is not sensitive to the tensile softening curve.

Key words: Concrete, Fracture, Initial toughness, Unstable toughness, Wedge splitting tests
doi:10.1631/jzus.A1300261   **Document code:** A   **CLC number:** TU528.1

1 Introduction

A large number of experimental studies on concrete fracture have shown that an obvious fracture process zone (FPZ) exists at the crack tip (Bazant and Planas, 1998). The traditional linear elastic fracture mechanics (LEFM), is no longer applicable to the analysis of the concrete fracture process (Jenq and Shah, 1985a) when the size of FPZ is comparable to the structure. To date, numerous nonlinear models for concrete fracture have been developed from different perspectives and based on various assumptions. The primary models and their characteristics are briefly summarized herein.

The fictitious crack model (FCM) (Hillerborg *et al.*, 1976) and crack band model (CBM) (Bazant and Oh, 1983) both considering the softening relation in the FPZ, were primarily solved numerically. The size effect law (SEL) developed by Bazant (1984) analyzes the size effect of the fracture by comparing nominal stress in the failure of structures with different sizes. The effective crack model (ECM) (Karihaloo and Nallathambi, 1990), known as the equivalent LEFM, has an explicit analytical solution. The two-parameter fracture model (TPFM) proposed by Jenq and Shah (1985a) was based on the assumption that crack propagation starts when the stress intensity factor and crack tip opening displacement (CTOD)

reach their critical values. The critical stress intensity factor K_{IC}^S in both ECM and TPFM was calculated from the peak load P_{max} and critical effective crack length a_c using a formula developed in LEFM.

Three different stages in the concrete fracture processes have been identified, namely, crack initiation, stable crack propagation, and unstable crack propagation (Xu and Reinhardt, 1999a). To depict the three stages of crack propagation without compromising simplicity, Xu and Reinhardt (1999a) developed the double-K model, which employed the initial toughness K_{IC}^{ini} and the unstable toughness K_{IC}^{un} as control parameters of the two important instantaneous states of crack initiation and instability, respectively. Macroscopic damage in concrete is believed to be initiated once the stress intensity factor at the crack tip reaches K_{IC}^{ini} (Zhang and Xu, 2011). Crack instability is the catastrophic point between the stable and unstable crack propagation stages and is significant in investigating the mechanisms of concrete fracture. The double-K model has been playing an important role in engineering practice. For instance, K_{IC}^{ini} and K_{IC}^{un} have been used in safety warning systems (DL/T 5332-2005, 2006) and in evaluating the performance of concrete structures with cracks.

The initial toughness K_{IC}^{ini} can be easily obtained using formulae of the initial cracking load and initial crack length based on LEFM (Xu and Reinhardt, 1999a). Several measurement methods for the initial cracking load, such as tests using photo-elastic coating, laser speckle (Xu and Reinhardt, 1999a) and strain gauge (Zhang and Xu, 2011), and analytical methods have been formulated. Xu and Reinhardt (1999b; 1999c; 2000) proposed the double-K method and developed a simplified method later. Kumar and Barai (2009) developed a weight function method. The comparison of the above analytical methods can be found in (Zhang and Xu, 2011). Recently, Qing and Li (2013) proposed a theoretical method to obtain K_{IC}^{ini} based on experimental peak load. Alternatively, as an easy method, Reinhardt and Xu (1999) and Zhang et al. (2010) determined the initial cracking load by the transition point that separates the linear and nonlinear segments of the load P-CMOD (crack mouth opening displacement) curve.

Nevertheless, predicting the unstable toughness K_{IC}^{un} is difficult without making any assumption. In the experimental aspect, K_{IC}^{un} can be calculated by the peak load P_{max} and the critical effective crack length a_c, which were mainly measured at the peak load state through the three point bending (TPB) specimens or wedge splitting (WS) specimens (DL/T 5332-2005, 2006). However, the critical effective crack length a_c was usually difficult to measure accurately. In traditional methods, a_c was calculated by critical crack mouth opening displacement $CMOD_c$ through empirical formulae (Xu and Reinhardt, 1999b; 1999c; Kumar and Barai, 2009; Zhang and Xu, 2011). Furthermore, in the numerical aspect, a similar step-by-step procedure must be followed until the maximum load was reached (Wu et al. 2007; Dong et al., 2013). Therefore, it is of significance to establish a simple theoretical method for predicting the unstable toughness K_{IC}^{un}.

Based on the analysis of concrete fracture mechanisms, the current study attempts to develop an easy-to-use theoretical method for predicting the unstable toughness K_{IC}^{un}. In this method, the initial toughness K_{IC}^{ini} was adopted as the control parameter of crack propagation and a weight function method was used to calculate the stress intensity factor and the crack opening displacement caused by the cohesive stress. Then the proposed method was verified using experimental data on wedge splitting specimens. The sensitivity of the results to the tensile softening curve was discussed.

2 Model development

2.1 Fracture processes of concrete

As mentioned in the previous section, the fracture processes in concrete structures include three different stages: crack initiation, stable crack propagation, and unstable fracture. To identify the three different states, the cohesive crack model with crack tip singularity (Elices and Planas, 1991) was adopted in the present work. Fig. 1 shows the different characteristics of the three stages, including the initial crack length a_0, crack propagation length Δa, external
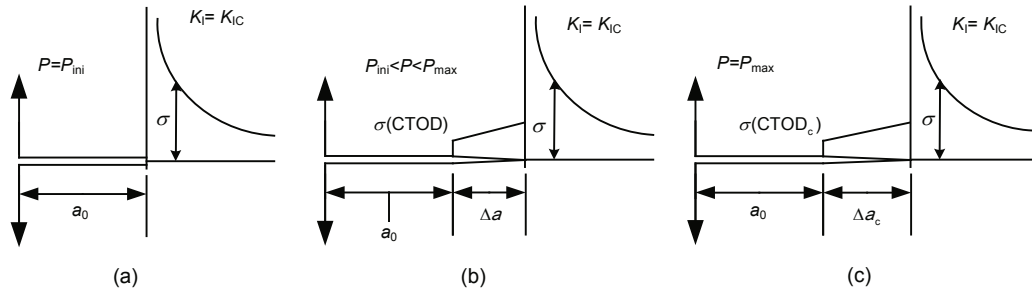
Fig. 1 Three stages of the concrete fracture processes
(a) Crack initiation; (b) Stable crack growth; (c) Unstable fracture

load P, stress strength factor K_I, and fracture toughness K_{IC}. Take type I load for example. When concrete is subjected to monotonic loading, cracks will not propagate until the external load P reaches the crack initiation load P_{ini} ($P=P_{ini}$), and $K_I = K_{IC}^{ini}$ (Fig. 1a). After crack initiation and as the external load P continuously increases, the crack starts to propagate, and a cohesive zone forms ahead of the initial crack, as shown in Fig. 1b. This period is commonly known as the stable crack propagation stage. Then the external load P reaches the peak (critical) value P_{max} (Fig. 1c). After that, unstable crack propagation may occur and the external load P decreases.

A typical P-a/D (a is the effective crack length, and D is the specimen height) curve is shown in Fig. 2 (Reinhardt and Xu, 1999; Kumar and Barai, 2008; Qing and Li, 2013). When P reaches the initial cracking load P_{ini}, crack begins to grow and it gradually and nonlinearly increases with a. When P reaches the peak load P_{max}, $a=a_c$. Then P gradually decreases with a. The derivation of P to a at $P=P_{max}$ can be assumed to be continuous (Qing and Li, 2013). The maximum theory can also be adopted to predict the crack instability.

2.2 Criterion for concrete fracture

As discussed above, a crack is initiated in concrete once the external load reaches the crack load P_{ini} or the stress intensity factor increases to the initial toughness K_{IC}^{ini}. Thus, K_{IC}^{ini} can be regarded as the toughness of the structural material to crack growth attributable to external forces. In the present study, the following criterion for crack initiation and propagation was employed (Xu and Reinhardt, 1999a; Wu
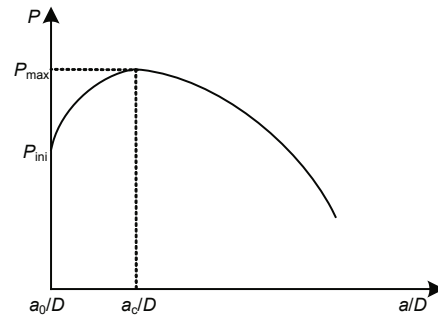

Fig. 2 A typical P-a/D curve of concrete fracture (Qing and Li, 2013)

et al., 2007; Dong *et al.*, 2013):

$$K_I = K_{IC}^{ini}, \tag{1}$$

where K_I is the stress intensity factor at the tip of the effective crack tip in a mode I fracture.

Before crack initiation, LEFM can be applied, and K_I can be calculated by

$$K_I = K_I^P, \tag{2a}$$

where K_I^P is the stress intensity factor attributable to the external load in a mode I fracture.

After the crack initiation, K_I can be expressed by the superposition scheme:

$$K_I = K_I^P + K_I^C, \tag{2b}$$

where K_I^C is the stress intensity factor attributable to cohesive stress.

2.3 Cohesive stress distribution

It is assumed that the cohesive stress distribution on the FPZ can be expressed by Eq. (3) (Li *et al.*, 2012). The cohesive stress at the tip of the effective crack equals the tensile strength. The cohesive stress at the tip of the initial crack and the crack tip opening displacement CTOD satisfy the tensile softening curve.

$$\sigma(b) = \sigma_s + (f_t - \sigma_s)\left(\frac{x - a_0}{a - a_0}\right)^m, \qquad (3)$$

where σ_s is the stress on the initial crack tip, f_t is the tensile strength, and m is the cohesion distribution index.

According to Eq. (3), the distribution of cohesive stress changes with the index m. When $m=1$, the cohesive stress distribution is linear. Eq. (3) is similar to the cohesive force distribution adopted by Reinhardt (1985). The difference is that the cohesive stress at the initial crack tip is not zero in the present model. Based on the theoretical model, the corresponding analytical approach is developed in the following section.

3 Analytical method for fracture

Take the WS specimen for example, the configuration of the WS specimen is shown in Fig. 3 (DL/T 5332-2005, 2006).

Fig. 3 Test set-up of WS specimen (DL/T 5332-2005, 2006)

$K_{\mathrm{I}}^{\mathrm{P}}$ can be expressed by (Xu and Reinhardt, 1999c):

$$K_{\mathrm{I}}^{\mathrm{P}} = \frac{P}{B\sqrt{D}} k(\alpha), \qquad (4)$$

where $\alpha = a/D$, and $k(\alpha)$ is a geometric factor, which can be calculated by (DL/T 5332-2005, 2006):

$$k(\alpha) = \frac{3.675\left[1 - 0.12(\alpha - 0.45)\right]}{(1 - \alpha)^{3/2}}. \qquad (5)$$

Eq. (5) is valid for $0.2 \leq \alpha \leq 0.8$ with 2% accuracy (Xu and Reinhardt, 1999c).

To obtain the value of $K_{\mathrm{I}}^{\mathrm{C}}$, a distribution of cohesive stress is assumed on the fictitious crack in an infinite strip (Jenq and Shah, 1985b). Previous studies have shown that the descending segment of the *P*-CMOD curve is affected by the cohesive stress distribution, while the peak load and critical crack mouth opening displacement are almost not affected (Li *et al.*, 2012). Therefore, to simplify the analysis of the fracture processes, a linear cohesive stress assumption ($m=1$) was adopted for the propagation state of concrete cracks in the current study. The cohesive stress distribution is shown in Fig. 4, where σ_s(CTOD) is the function of CTOD.
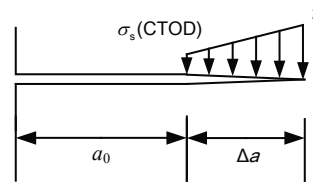
Fig. 4 Linear distribution of cohesive stress

The weight function method proposed by Kumar and Barai (2009) was adopted in this study to calculate $K_{\mathrm{I}}^{\mathrm{C}}$:

$$K_{\mathrm{I}}^{\mathrm{C}} = \frac{2}{\sqrt{2\pi a}} g(a), \qquad (6)$$

where $g(a)$ can be expressed using the following fourth-order weight function:

$$g(a) = A_{\mathrm{l}} a \left(2s^{1/2} + M_1 s + \frac{2}{3} M_2 s^{3/2} + \frac{M_3}{2} s^2 \right)$$

$$+ A_2 a^2 \left[\frac{4}{3} s^{3/2} + \frac{M_1}{2} s^2 + \frac{4}{15} M_2 s^{5/2} \right.$$
$$\left. + \frac{M_3}{6} \left(1 - \left(\frac{a_0}{a} \right)^3 - 3s \frac{a_0}{a} \right) \right], \tag{7}$$

where $A_1 = \sigma_s(\text{CTOD})$, $A_2 = [f_t - \sigma(\text{CTOD})]/(a - a_0)$, $s = 1 - a_0/a$, M_1, M_2, and M_3 can be expressed by α (Kumar and Barai, 2009).

The CTOD and $\sigma_s(\text{CTOD})$ values are required to calculate K_I^C using Eqs. (6) and (7), where $\sigma_s(\text{CTOD})$ can be expressed by (Reinhardt $et\ al.$, 1986):

$$\sigma_s(\text{CTOD}) = f_t \left\{ \left[1 + \left(\frac{c_1 \text{CTOD}}{w_0} \right)^3 \right] \exp \left(\frac{-c_2 \text{CTOD}}{w_0} \right) \right.$$
$$\left. - \frac{\text{CTOD}}{w_0} (1 + c_1^3) \exp(-c_2) \right\}, \tag{8}$$

where c_1, c_2, and w_0 are parameters.

CTOD in Eq. (8) needs to be calculated by adding up two displacements caused by the external load P and cohesive stress. Using Paris' displacement formula (Tada $et\ al.$, 2000; Mai, 2002), CTOD can be expressed by

$$\text{CTOD} = \frac{2}{E} \int_{a_0}^{a} \frac{P}{B\sqrt{D}} k \left(\frac{\xi}{D} \right) m(a_0, \xi) \mathrm{d}\xi$$
$$- \frac{2}{E} \int_{a_0}^{a} \frac{2}{\sqrt{2\pi\xi}} g(\xi) m(\xi, a) \mathrm{d}\xi, \tag{9}$$

where E is the elasticity modules, ξ is the integration variable, $m(x, a)$ can be expressed using the following fourth-order weight function (Kumar and Barai, 2009):

$$m(x, a) = \frac{2}{\sqrt{2\pi(a-x)}} \left[1 + M_1 \left(1 - \frac{x}{a} \right)^{1/2} \right.$$
$$\left. + M_2 \left(1 - \frac{x}{a} \right) + M_3 \left(1 - \frac{x}{a} \right)^{3/2} \right]. \tag{10}$$

Thus, using Eqs. (7)–(9), $g(a)$ can be derived, and K_I^C can be obtained using Eq. (6). Then, substi-tuting Eq. (4) for K_I^P and Eq. (6) for K_I^C into Eq. (2b) leads to:

$$P = \zeta(a) + \eta(a) K_{\text{IC}}^{\text{ini}}, \tag{11}$$

where

$$\zeta(a) = \frac{2B\sqrt{D}}{\sqrt{2\pi a} k(\alpha)} g(a),$$
$$\eta(a) = B\sqrt{D} \frac{1}{k(\alpha)}.$$

Eq. (11) obviously shows that the external load P can be explicitly expressed as a function of the effective crack length a. The derivation of this equation with respect to a at the moment of the crack instability can be expressed by the following partial differential equation:

$$\left. \frac{\partial P}{\partial a} \right|_{a=a_c} = 0, \tag{12}$$

and $\frac{\partial P}{\partial a}$ is calculated by

$$\frac{\partial P}{\partial a} = \zeta'(a) + \eta'(a) K_{\text{IC}}^{\text{ini}}, \tag{13}$$

where

$$\zeta'(a) = \frac{2B\sqrt{D}}{\sqrt{2\pi}} \frac{g'(a)k(\alpha)\sqrt{a} - g(a) \left[k'(a)\sqrt{a} + \frac{k(\alpha)}{2\sqrt{a}} \right]}{k^2(\alpha) a},$$
$$\eta'(a) = -B\sqrt{D} \frac{k'(\alpha)}{k^2(\alpha)}.$$

$g'(a)$ can be expressed as

$$g'(a) = (A_1 + A_1'a) \left(2s^{1/2} + M_1 s + \frac{2}{3} M_2 s^{3/2} + \frac{M_3}{2} s^2 \right)$$
$$+ A_1 a (s^{-1/2} + M_1 + M_2 s^{1/2} + M_3 s)s'$$
$$+ A_2 a^2 \left[\left(2s^{1/2} + M_1 s + \frac{2}{3} M_2 s^{3/2} \right) s' \right.$$
$$\left. + \frac{M_3}{2} \left(\frac{a_0^3}{a^4} - s' \frac{a_0}{a} + s \frac{a_0}{a^2} \right) \right]$$

$$+(2A_2 a + A_2' a^2)\left[\frac{4}{3}s^{3/2} + \frac{M_1}{2}s^2\right.$$
$$\left.+\frac{4}{15}M_2 s^{5/2} + \frac{M_3}{6}\left(1-\left(\frac{a_0}{a}\right)^3 - 3s\frac{a_0}{a}\right)\right],$$
(14)

where

$$s' = \frac{a_0}{a^2},$$

$$A_1' = \frac{\partial \sigma_s(\text{CTOD})}{\partial a} = \frac{\partial \sigma_s(\text{CTOD})}{\partial \text{CTOD}}\frac{\partial \text{CTOD}}{\partial a},$$

$$A_2' = \frac{-\sigma_s'(\text{CTOD})(a-a_0)-[f_t-\sigma_s(\text{CTOD})]}{(a-a_0)^2}.$$

$k'(\alpha)$ can be expressed as

$$k'(\alpha)$$
$$= \frac{-0.441(1-\alpha)^{3/2} + (5.810175 - 0.6615\alpha)(1-\alpha)^{1/2}}{(1-\alpha)^3}.$$
(15)

If the initial toughness $K_{\text{IC}}^{\text{ini}}$ is given, the critical effective crack length a_c can be calculated using Eq. (12) by iterating method. Then, the critical crack tip opening displacement CTOD_c and the peak load P_{max} can be obtained by substituting $a=a_c$ into Eq. (9) and Eq. (11), respectively. The unstable toughness $K_{\text{IC}}^{\text{un}}$ can be calculated by substituting $a=a_c$ and $P=$

P_{max} into Eq. (4). Hence, an analytical approach for calculating $K_{\text{IC}}^{\text{un}}$ was developed.

4 Results and discussion

4.1 Verification of the analytical method

In this section, the proposed method for concrete fracture was verified using the data from Xu et al. (2006)'s experiments on WS specimens with different maximum aggregate sizes. The parameters of the specimens are shown in Table 1. In the experiments, the crack initiation load P_{ini} was measured by resistance strain gauges and the initial toughness $K_{\text{IC}}^{\text{ini}}$ was obtained by the LEFM formula.

According to the experimental conditions, the parameters in Eq. (8) for the proposed method were taken as follows: $c_1=3$, $c_2=6.93$, and $w_0=160$ μm (Reinhardt et al., 1986).

The calculated and measured values of the peak load P_{max} are compared in Tables 2–4. It can be seen from the comparison that the values of the peak load P_{max} calculated by the proposed method are generally in good agreement with the experimental values for different maximum aggregate sizes of concrete specimens. It can be concluded that the method is effective for predicting the instability of concrete.

Moreover, the values of unstable toughness $K_{\text{IC}}^{\text{un}}$

Table 1 Parameters of the wedge splitting specimens

Specimen No.	Specimen size, $2H \times D \times B$ (mm)	Maximum aggregate size (mm)	a_0 (mm)	E (GPa)	Compressive strength, f_c (MPa)	Tensile strength, f_t (MPa)
WS13	300×300×200	20	150	33.4	34.2	2.76
WS14	600×600×200	20	300	33.4	34.2	2.76
WS15	800×800×200	20	400	33.4	34.2	2.76
WS16	1000×1000×200	20	500	33.4	34.2	2.76
WS17	1200×1200×200	20	600	33.4	34.2	2.76
WS32	300×300×200	40	150	29.1	34.3	3.04
WS22	600×600×200	40	300	29.1	34.3	3.04
WS34	800×800×200	40	400	29.1	34.3	3.04
WS35	1000×1000×200	40	500	29.1	34.3	3.04
WS23	600×600×250	80	300	29.1	34.3	3.04
WS24	800×800×250	80	400	29.1	34.3	3.04
WS25	1000×1000×250	80	500	29.1	34.3	3.04
WS26	1200×1200×250	80	600	29.1	34.3	3.04

Table 2 Comparison of the predicted and measured results (maximum aggregate size: 20 mm)

Specimen No.	Specimen size, $2H{\times}D{\times}B$ (mm)	a_0 (mm)	P_{ini} (kN)	Predicted a_c/D	Predicted P_{max} (kN)	Experimental P_{max} (kN)	Predicted K_{IC}^{un} (1)	Experimental K_{IC}^{un} (2)	(1)/(2)
WS13-1	300×300×200	150	7.181	0.620	11.668	12.173	1.637	1.690	0.969
WS13-2	300×300×200	150	10.916	0.567	14.156	12.801	1.642	1.958	0.838
WS13-4	300×300×200	150	7.909	0.607	12.095	11.492	1.614	1.759	0.918
Mean			8.669	0.598	12.639	12.155	1.631	1.802	0.908
WS14-1	600×600×200	300	19.308	0.569	25.387	25.550	2.098	2.224	0.943
WS14-2	600×600×200	300	18.484	0.583	24.787	22.667	2.148	2.462	0.872
WS14-4	600×600×200	300	18.000	0.583	24.437	23.408	2.117	2.004	1.057
Mean			18.597	0.578	24.870	23.875	2.121	2.230	0.957
WS15-1	800×800×200	400	23.788	0.597	32.848	30.758	2.596	2.191	1.185
WS15-2	800×800×200	400	24.546	0.584	33.387	31.136	2.511	2.135	1.176
WS15-3	800×800×200	400	17.403	0.639	28.776	29.351	2.667	2.102	1.269
Mean			21.912	0.607	31.670	30.415	2.591	2.143	1.210
WS16-1	1000×1000×200	500	32.495	0.570	42.677	42.137	2.741	2.974	0.922
WS16-2	1000×1000×200	500	30.478	0.584	41.205	39.000	2.777	2.851	0.974
WS16-3	1000×1000×200	500	24.235	0.612	36.929	31.494	2.753	2.250	1.224
Mean			29.069	0.589	40.270	37.544	2.757	2.692	1.040
WS17-1	1200×1200×200	600	33.368	0.584	46.734	46.326	2.878	3.231	0.891
WS17-2	1200×1200×200	600	36.699	0.584	49.142	55.183	3.026	3.028	0.999
WS17-3	1200×1200×200	600	40.045	0.570	51.689	50.355	3.033	3.112	0.975
Mean			36.704	0.579	49.188	50.621	2.979	3.124	0.955

Table 3 Comparison of the predicted and measured results (maximum aggregate size: 40 mm)

Specimen No.	Specimen size, $2H{\times}D{\times}B$ (mm)	a_0 (mm)	P_{ini} (kN)	Predicted a_c/D	Predicted P_{max} (kN)	Experimental P_{max} (kN)	Predicted K_{IC}^{un} (1)	Experimental K_{IC}^{un} (2)	(1)/(2)
WS32-1	300×300×200	150	8.234	0.593	12.237	11.221	1.556	1.524	1.021
WS32-2	300×300×200	150	8.848	0.580	11.384	9.433	1.381	1.232	1.121
WS32-3	300×300×200	150	8.431	0.593	12.366	10.727	1.572	1.371	1.147
Mean			8.504	0.589	11.996	10.460	1.503	1.376	1.096
WS33-2	600×600×200	300	18.973	0.569	25.017	24.511	2.068	1.957	1.057
WS33-3	600×600×200	300	18.588	0.569	24.725	21.956	2.044	2.132	0.959
WS33-4	600×600×200	300	16.091	0.583	22.912	21.242	1.985	2.006	0.990
Mean			17.884	0.574	24.218	22.570	2.032	2.032	1.002
WS34-1	800×800×200	400	22.306	0.584	30.683	27.349	2.308	2.016	1.145
WS34-2	800×800×200	400	18.766	0.597	28.215	27.049	2.230	2.106	1.059
WS34-4	800×800×200	400	26.711	0.570	34.006	32.000	2.439	2.713	0.899
Mean			22.594	0.584	30.968	28.799	2.326	2.278	1.034
WS35-2	1000×1000×200	500	21.337	0.598	33.364	29.866	2.363	2.071	1.141
WS35-3	1000×1000×200	500	19.284	0.612	32.076	25.634	2.391	1.884	1.269
WS35-4	1000×1000×200	500	21.837	0.598	33.698	32.700	2.386	2.336	1.021
Mean			20.819	0.603	33.046	29.400	2.380	2.097	1.144

Table 4 Comparison of the predicted and measured results (maximum aggregate size: 80 mm)

Specimen No.	Specimen size, $2H{\times}D{\times}B$ (mm)	a_0 (mm)	P_{ini} (kN)	Predicted a_c/D	Predicted P_{max} (kN)	Experimental P_{max} (kN)	Predicted K_{IC}^{un} (1)	Experimental K_{IC}^{un} (2)	(1)/(2)
WS23-2	600×600×250	300	16.525	0.638	27.138	23.407	2.312	2.465	0.938
WS23-4	600×600×250	300	17.451	0.624	27.675	24.340	2.233	2.260	0.988
Mean			16.988	0.631	27.407	23.874	2.273	2.363	0.963
WS24-1	800×800×250	400	29.425	0.584	40.357	36.833	2.429	2.867	0.847
WS24-3	800×800×250	400	31.575	0.584	41.924	35.859	2.523	2.385	1.058
WS24-4	800×800×250	400	19.594	0.639	34.058	32.178	2.525	2.766	0.913
Mean			26.865	0.602	38.780	34.957	2.492	2.673	0.939
WS25-1	1000×1000×250	500	25.000	0.626	42.102	43.711	2.649	2.814	0.941
WS25-2	1000×1000×250	500	34.093	0.584	48.006	45.163	2.588	3.043	0.850
WS25-4	1000×1000×250	500	20.590	0.640	39.637	39.194	2.636	2.308	1.142
Mean			26.561	0.617	43.248	42.689	2.624	2.722	0.978
WS26-1	1200×1200×250	600	45.168	0.570	60.206	54.000	2.826	2.931	0.964
WS26-2	1200×1200×250	600	37.663	0.598	54.773	47.340	2.836	3.326	0.853
Mean			41.416	0.584	57.490	50.670	2.831	3.129	0.909

are also shown in Tables 2–4. The calculated values of K_{IC}^{un} by the proposed method generally agree well with those by experimental method. Some of the calculated results are slightly different from those obtained by the experimental method, for example, the ratio of the predicted result to experimental result of WS15 is 1.21. According to Eq. (4), the discrepancy in the unstable toughness results from the critical relative effective crack length a_c/D. The primary reason is that, as mentioned above, an empirical formula was adopted in the experimental method to calculate the critical effective length a_c. The proposed method, differing from the experimental method, is capable of considering the effects of both external load and cohesive force when calculating a_c.

4.2 Effect of tensile softening curve

To study the sensitivity of the method to the shape of the tensile softening curve, two groups of parameters characterizing different tensile softening curves were used to predict fracture using the proposed theoretical method.

The parameters of first group were $c_1{=}3$, $c_2{=}6.93$, and $w_0{=}160$ μm, which were adopted in the last section. For comparison, the second set of the softening curve parameters was taken as as $c_1{=}1.5$, $c_2{=}6.3$, and $w_0{=}90$ μm. The tensile softening curves represented by these two sets of parameters are shown in Fig. 5.

With these different parameters, the values of P_{max}, a_c/D, and K_{IC}^{un} were calculated using the proposed method, and the results are shown in Figs. 6–8. As can be seen from Figs. 6–8, the calculated P_{max}, a_c/D, and K_{IC}^{un} using the first group of parameters are slightly different from those of the other one. Generally, this disparity in the calculated results using these two sets of parameters is considered to be insignificant in view of the great difference between the two tensile softening curves. For example, the fracture energy G_F (area under the tensile softening curve) corresponding to the first softening curve is about twice that for the second one.
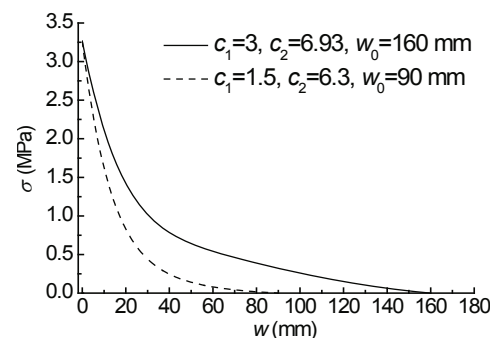

Fig. 5 Tensile softening curves

5 Conclusions

In this study, the instability state of fracture in concrete was predicted by a theoretical model which

adopted the initial toughness K_{IC}^{ini} as the crack propagation criterion, and used the weight function method to calculate the stress intensity factor and the crack opening displacement caused by the cohesive stress. The applicability of the proposed method was verified by experimental data obtained on WS specimens, and the parameters at the peak load state, such as the peak load P_{max}, critical effective crack length a_c and unstable toughness K_{IC}^{un}, were calculated using the proposed method. The good agreement between the calculated results and the experimental results demonstrates that the proposed method can accurately predict the unstable toughness K_{IC}^{un}. In addition, the sensitivity of the results to the tensile softening curve was discussed. The results showed that the proposed method for fracture is not sensitive to the tensile softening curve, which verifies the reasonability of the proposed method. Future studies can be conducted from many aspects, such as the investigation of measurement methods for the effective crack length a_c.
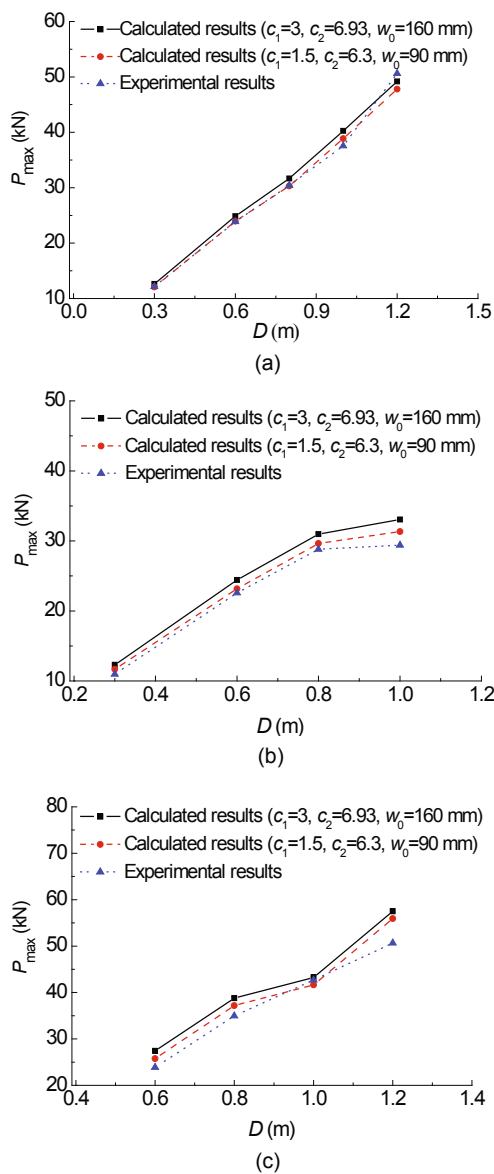

Fig. 6 Average values of P_{max} for specimens with different maximum aggregate sizes of 20 mm (a), 40 mm (b), and 80 mm (c)
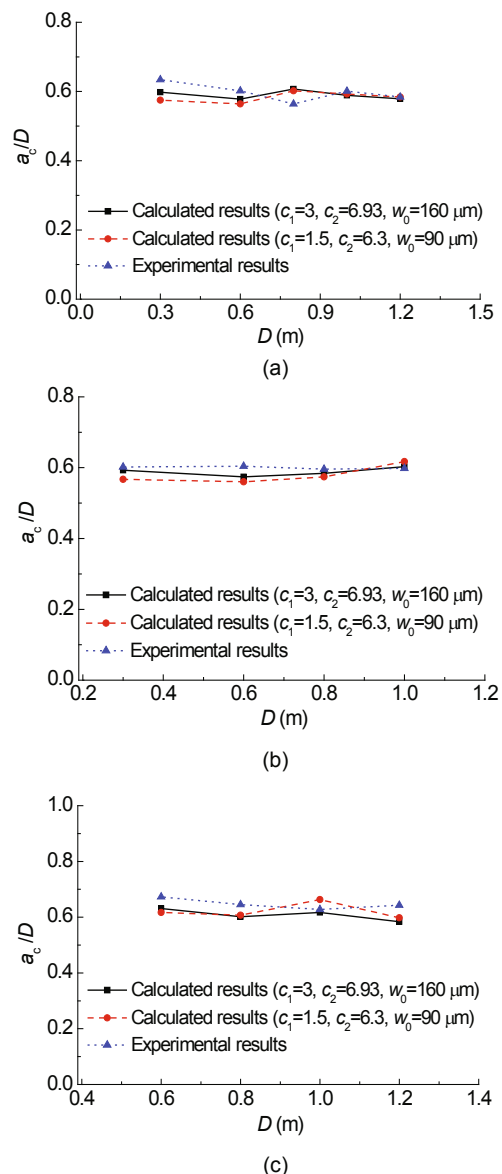

Fig. 7 Average values of a_c/D for specimens with different maximum aggregate sizes of 20 mm (a), 40 mm (b), and 80 mm (c)
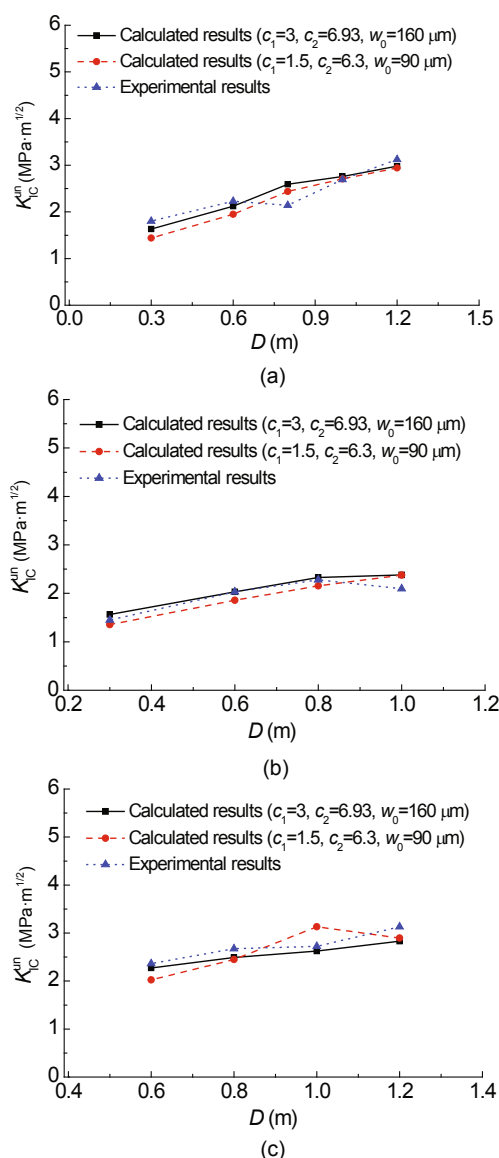
Fig. 8 Average values of K_{IC}^{un} for specimens with different maximum aggregate sizes of 20 mm (a), 40 mm (b), and 80 mm (c)

References

Bazant, Z.P., 1984. Size effect in blunt fracture: concrete, rock, metal. *Journal of Engineering Mechanics*, **110**(4):518-535. [doi:10.1061/(ASCE)0733-9399(1984)110:4(518)]

Bazant, Z.P., Oh, B.H., 1983. Crack band theory for fracture of concrete. *Material and Structure*, **16**(3):155-177. [doi:10.1007/BF02486267]

Bazant, Z.P., Planas, J., 1998. Fracture and Size Effect in Concrete and Other Quasibrittle Materials. CRC Press, Boca Raton.

DL/T 5332-2005, 2006. Specification for Fracture Test of Hydraulic Concrete. China Electric Power Press, Beijing, China (in Chinese).

Dong, W., Wu, Z.M., Zhou, X.M., 2013. Calculating crack extension resistance of concrete based on a new crack propagation criterion. *Construction and Building Materials*, **38**:879-889. [doi:10.1016/j.conbuildmat.2012.09.037]

Elices, M., Planas, J., 1991. Material models. *In*: Elfgren, L. (Ed.), Fracture Mechanics of Concrete Structures from Theory to Applications. Report of RILEM Technical Committee 90-FMT. Chapman & Hall, London, p.16-65.

Hillerborg, A., Modeer, M., Petersson, P.E., 1976. Analysis of crack formation crack growth in concrete by means of fracture mechanics and finite elements. *Cement and Concrete Research*, **6**(6):773-782. [doi:10.1016/0008-8846(76)90007-7]

Jenq, Y.S., Shah, S.P., 1985a. Two parameter fracture model for concrete. *Journal of Engineering Mechanics*, **111**(10):1227-1241. [doi:10.1061/(ASCE)0733-9399(1985)111:10(1227)]

Jenq, Y.S., Shah, S.P., 1985b. A fracture toughness criterion for concrete. *Engineering Fracture Mechanics*, **21**(5):1055-1069. [doi:10.1016/0013-7944(85)90009-8]

Karihaloo, B.L., Nallathambi, P., 1990. Effective cracks model for the determination of fracture toughness (KICS) of concrete. *Engineering Fracture Mechanics*, **35**(4-5):637-645. [doi:10.1016/0013-7944(90)90146-8]

Kumar, S., Barai, S.V., 2008. Influence of specimen geometry and size-effect on the K_R-curve based on the cohesive stress in concrete. *International Journal of Fracture*, **152**(2):127-148. [doi:10.1007/s10704-008-9275-6]

Kumar, S., Barai, S.V., 2009. Determining double-K fracture parameters of concrete for compact tension and wedge splitting tests using weight function. *Engineering Fracture Mechanics*, **76**(7):935-948. [doi:10.1016/j.engfracmech.2008.12.018]

Li, Q.B., Qing, L.B., Guan, J.F., 2012. Analysis of the whole fracture process of concrete considering effects of cohesive distribution. *Journal of Hydraulic Engineering*, **43**(Sup.):31-36 (in Chinese).

Mai, Y.W., 2002. Cohesive zone and crack-resistance (*R*)-curve of cementitious materials and their fibre-reinforced composites. *Engineering Fracture Mechanics*, **69**(2):219-234. [doi:10.1016/S0013-7944(01)00086-8]

Qing, L.B., Li, Q.B., 2013. A theoretical method for determining initiation toughness based on experimental peak load. *Engineering Fracture Mechanics*, **99**:295-305. [doi:10.1016/j.engfracmech.2013.01.012]

Reinhardt, H.W., 1985. Plain concrete modeled as an elastic strain-softening material at fracture. *Engineering Fracture Mechanics*, **22**(5):787-796. [doi:10.1016/0013-7944(85)90108-0]

Reinhardt, H.W., Xu, S.L., 1999. Crack extension resistance based on the cohesive force in concrete. *Engineering Fracture Mechanics*, **64**(5):563-587. [doi:10.1016/S0013-7944(99)00080-6]

Reinhardt, H.W., Cornelissen, H.A.W., Hordijk, D.A., 1986. Tensile tests and failure analysis of concrete. *Journal of Structural Engineering*, **112**(11):2462-2477. [doi:10.1061/(ASCE)0733-9445(1986)112:11(2462)]

Tada, H., Paris, P.C., Irwin, G., 2000. The Stress Analysis of Cracks Handbook, Third Edition. New York.

Wu, Z.M., Dong, W., Liu, K., Yang, S.T., 2007. Mode I crack propagation criterion of concrete and numerical simulation on complete process of cracking. *Journal of Hydraulic Engineering*, **38**:46-52 (in Chinese).

Xu, S.L., Reinhardt, H.W., 1999a. Determination of double-*K* criterion for crack propagation in quasi-brittle fracture, Part I: experimental investigation of crack propagation. *International Journal of Fracture*, **98**(2):111-149. [doi:10.1023/A:1018668929989]

Xu, S.L., Reinhardt, H.W., 1999b. Determination of double-*K* criterion for crack propagation in quasi-brittle fracture, Part II: analytical evaluating and practical measuring methods for three-point bending notched beams. *International Journal of Fracture*, **98**(2):151-177. [doi:10.1023/A:1018740728458]

Xu, S.L., Reinhardt, H.W., 1999c. Determination of double-*K* criterion for crack propagation in quasi-brittle fracture, Part III: compact tension specimens and wedge splitting specimens. *International Journal of Fracture*, **98**(2):179-193. [doi:10.1023/A:1018788611620]

Xu, S.L., Reinhardt, H.W., 2000. A simplified method for determining double-K fracture parameters for three-point bending tests. *International Journal of Fracture*, **104**(2):181-209. [doi:10.1023/A:1007676716549]

Xu, S.L., Zhou, H.G., Gao, H.B., Zhao, S.Y., 2006. An experimental study on double-K fracture parameters of concrete for dam construction with various grading aggregates. *China Civil Engineering Journal*, **39**(11):50-62.

Zhang, J., Leung, K.Y., Xu, S.L., 2010. Evaluation of fracture parameters of concrete from bending test using inverse analysis approach. *Materials and Structure*, **43**(6):857-875. [doi:10.1617/s11527-009-9552-5]

Zhang, X.F., Xu, S.L., 2011. A comparative study on five approaches to evaluate double-K fracture toughness parameters of concrete and size effect analysis. *Engineering Fracture Mechanics*, **78**(10):2115-2138. [doi:10.1016/j.engfracmech.2011.03.014]

中文概要：

本文题目：基于起裂韧度准则的混凝土失稳韧度预测研究

Predicting unstable toughness of concrete based on initial toughness criterion

研究目的：研究混凝土失稳韧度的理论预测方法。

创新要点：1. 提出混凝土失稳韧度的理论预测方法；2. 利用楔入劈拉试件计算不同级配混凝土的失稳韧度；3. 研究失稳韧度受拉伸软化曲线的影响。

研究方法：1. 基于起裂韧度扩展准则，采用理论分析手段研究混凝土的失稳韧度计算方法；2. 利用楔入劈拉试件（见图3）计算不同级配混凝土的失稳韧度。

重要结论：1. 基于起裂韧度准则可合理地预测峰值荷载状态及失稳韧度；2. 混凝土失稳韧度受断裂能的影响较小；3. 拉伸软化曲线对混凝土失稳韧度的影响较小。

关键词组：混凝土；起裂韧度；失稳韧度；楔入劈拉实验